SEVENTH SEMI-ANNUAL PROGRESS REPORT

NASA GRANT NAG8-790

PROCESS MODELLING FOR MATERIALS PREPARATION EXPERIMENTS

Period of Performance
8/1/92 through 1/31/93

Principal Investigator

FRANZ ROSENBERGER

Co-Principal Investigator

J. IWAN D. ALEXANDER

Center for Microgravity and Materials Research
University of Alabama in Huntsville
Huntsville, Alabama 35899

1. Introduction and General Status

The main goals of the research under this grant consist of the development of mathematical tools and measurement of transport properties necessary for high fidelity modelling of crystal growth from the melt and solution, in particular for the Bridgman-Stockbarger growth of mercury cadmium telluride (MCT) and the solution growth of triglycine sulphate (TGS). Of the tasks desribed in detail in the original proposal, two remain to be worked on:

- development of a spectral code for moving boundary problems,
- diffusivity measurements on concentrated and supersaturated TGS solutions.

During this seventh half-year period, good progress has been made on these tasks.

2. MCT Code development

In the last six-monthly report we described our work on the solution of the coupled equations governing momentum (fluid flow) and heat transport together with a moving boundary. We reported that the chief problems met during this period have been associated with excessively long iteration times and that a Preconditioned Generalized Conjugate Residual (PGCR) scheme had been implemented for an irregular domain with a fixed non-planar boundary in an attempt to alleviate this problem and that we would apply it to the moving boundary if appropriate.

We have since successfully implemented this scheme for the general moving boundary problem. Our method and the results of a careful comparison of our Bridgman code with other work is described in the attached paper which will be submitted for publication in the International Journal of Numerical Methods for Heat and Fluid Flow. In an attempt to demonstrate the portability of our code from the CRAY to workstations we have tested the performance of our code on a variety of machines. The results are also described in the paper. Work will continue on further development of the code to include a non-dilute dopant and to investigate the feasibility of incorporating radiation between the furnace and ampoule using a Finite Element approach.

3. Diffusivity Measurements

In the last report we had stated that the development of a new interferometric method to measure the diffusivities of supersaturated solutions had been completed. The method was described in that report as well as in earlier ones. A rectangular optical cell is initially filled with a solution of a certain concentration C. A solution of higher concentration $C + \Delta C$ is then injected at the bottom of the cell by means of a syringe. The resulting system is convectively stable, in one-dimensional terms, with the heavier solution below the lighter one and mixing

occurs by diffusion only. A Zygo Mark II Mach-Zehnder interferometer interfaced with a personal computer is used to follow the evolution of the concentration profile in the cell. At regular intervals the interferometric intensity profiles produced are stored and the advanced fringe analysis software ZAPPC is used to convert these into refractive index profiles which are proportional to the concentration. A numerical integration of these profiles yields the diffusivity.

Several measurements were done with undersaturated and supersaturated solutions of sodium chloride and some of these results were shown in our last report. Our method compares well with earlier measurements of diffusivity [1,2] and has a reproducability of better than 1% for undersaturated solutions. However, in the supersaturated region the only other attempt to measure diffusivities was done by Myerson and co-workers and our values are significantly lower than the value reported by them for sodium chloride. Their method, as are most other methods, is based on the assumption of constant diffusivity in the concentration range of the solution pair used in each measurement. In the supersaturated region the diffusivity is a strong function of the concentration and this assumption is no longer valid. Our method does not make such an assumption and this is probably the reason for the discrepancy between our values and theirs.

Diffusivity measurements were also made with TGS solutions at 25°C and these are shown in fig. 1. The crystalline TGS used to prepare the solutions were provided by Dr. Roger Kroes of NASA Marshall Space Flight Center. He also provided the original data from his diffusivity and refractive index measurements for undersaturated TGS solutions that were presented in graph form in his publications [3,4]. Solubility data for TGS solutions were also obtained from the literature [3,5,6]. The refractive index of supersaturated TGS solutions was needed for the diffusivity calculations and this was measured with a temperature controlled Milton Roy Abbe-3L refractometer.

We have shown that our method can be successfully used to measure the diffusivities of supersaturated TGS solutions at ambient temperatures. We are currently performing measurements at concentrations between those shon in fig. 1, in order to obtain a reliable curve for the concentration dependence of TGS diffusivities at 25°C. In the near future we will be designing a temperature controlled apparatus to measure diffusivities at other temperatures as well.

References

[1] J.A. Rard and D.G. Miller, *The Mutual Diffusion Coefficients of NaCl-H_2O and $CaCl_2$-H_2O at 25°C from Rayleigh Interferometry*, J. Solution Chem, **8** (1979) 701.

[2] Y.C. Chang and A.S. Myerson, *The Diffusivity of Potassium Chloride and Sodium Chloride in Concentrated, Saturated and Supersaturated Solutions,* AIChE J., **31** (1985) 890.

[3] R.L. Kroes and D. Reiss, *Properties of TGS Aqueous Solution for Crystal Growth,* J. Crystal Growth, **69** (1984) 414.

[4] S.H. Morgan, E. Silberman, R.L. Kroes and D. Reiss, *Raman Study of the Diffusion of Triglycine Sulfate in Aqueous Solutions,* Appl. Spectroscopy, **40** (1985) 35.

[5] B. Brezina, *Growth and Characterization of Solid Solutions of Ferroelectric TGS Single Crystals with Isomorphous Compounds,* Mat. Res. Bull., **6** (1971) 401.

[6] R.J. Davey and E.A.D. White, *Growth of Triglycine Sulphate Crystals from Aqueous Solutions on Cleaved (010) Surfaces,* J. Crystal Growth, **30** (1975) 125.

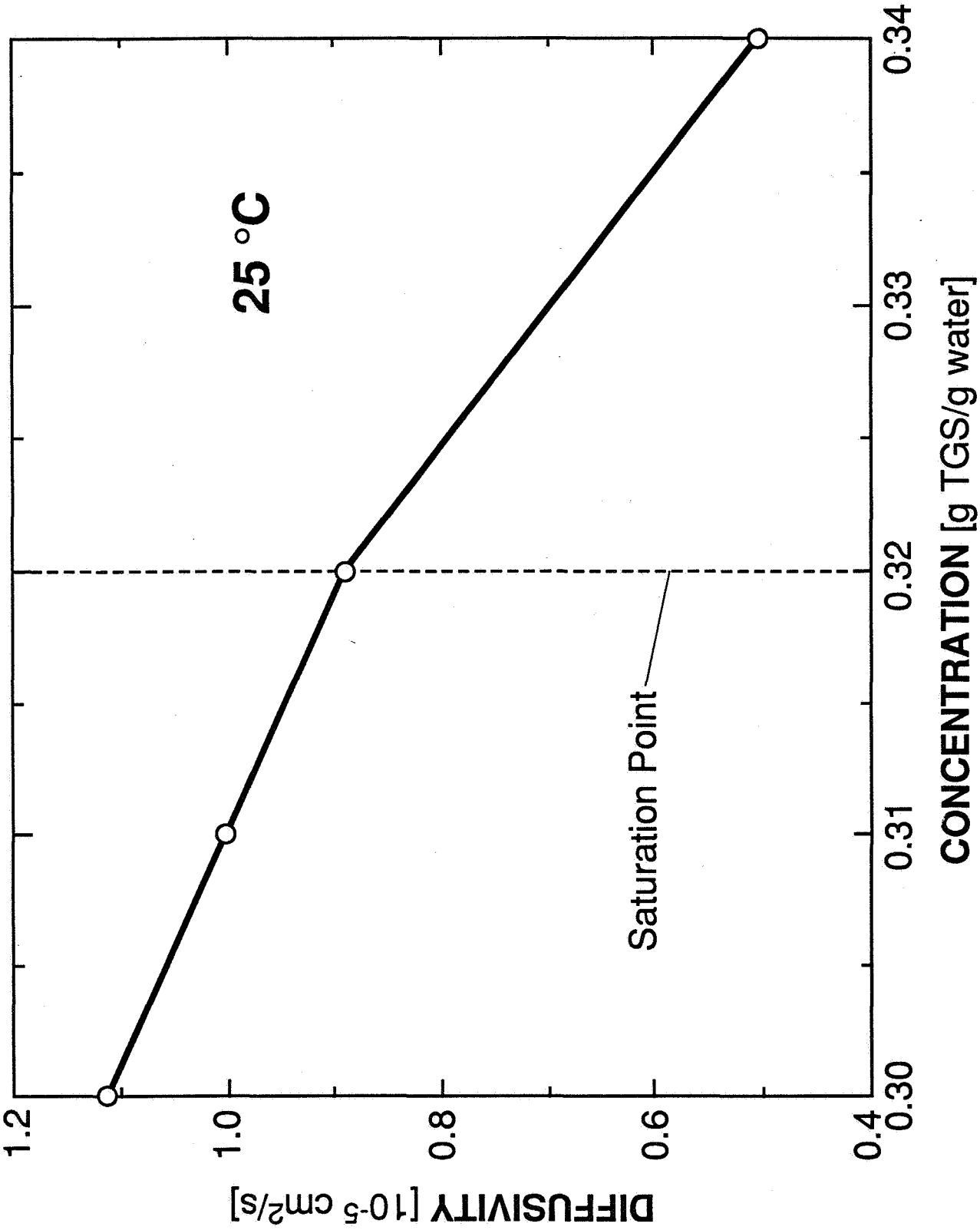
25 °C
Saturation Point
DIFFUSIVITY [10-5 cm2/s]
CONCENTRATION [g TGS/g water]
1.2
1.0
0.8
0.6
0.4
0.30
0.31
0.32
0.33
0.34

FIG. 1

4. Presentations and Publications

From the work carried out under this grant the following papers have been published, accepted for publication or are in preparation for submission for publication:

1. A. Nadarajah, F. Rosenberger and J. I. D. Alexander, *Modelling the Solution Growth of Triglycine Sulfate in Low Gravity,* J. Crystal Growth **104** (1990) 218-232.
2. F. Rosenberger, J. I. D. Alexander, A. Nadarajah and J. Ouazzani, Influence of Residual Gravity on Crystal Growth Processes, Microgravity Sci. Technol. **3** (1990) 162-164.
3. J. P. Pulicani and J. Ouazzani, *A Fourier-Chebyshev Pseudo-Spectral Method for Solving Steady 3-D Navier-Stokes and Heat Equations in Cylindrical Cavities*, Computers and Fluids **20** (1991) 93.
4. J. P. Pulicani, S. Krukowski, J. I. D. Alexander, J. Ouazzani and F. Rosenberger, *Convection in an Asymmetrically Heated Cylinder*, Int. J. Heat Mass Transfer **35** (192) 2119.
5. F. Rosenberger, J. I. D. Alexander and W.-Q. Jin, *Gravimetric Capillary Method for Kinematic Viscosity Measurements,* Rev. Sci. Instr. **63** (192) 269.
6. A. Nadarajah, F. Rosenberger and T. Nyce, *Interferometric Technique for Diffusivity Measurements in (Supersaturated) Solutions,* J. Phys. Chem (submitted).
7. F. Rosenberger, *Boundary Layers in Crystal Growth, Facts and Fancy*, in **Lectures on Crystal Growth,** ed. by H. Komatsu (in print).
8. F. Rosenberger, *Short-duration Low-gravity Experiments - Time Scales, Challenges and Results,* Microgravity Sci. Applic. (submitted).
9. Y. Zhang, J.I.D. Alexander and J. Ouazzani, *A Chebishev Collocation Method For Moving Boundaries, Heat Transfer and Convection During Directional Solidification,* Internat. J. Numerical Methods Heat Fluid Flow (in preparation).

In addition to the above publications, the results of our work have been presented at the following conferences and institutions:

1. J.I.D. Alexander, *Modelling the Solution Growth of TGS Crystals in Low Gravity,* Committee on Space Research (COSPAR) Plenary Meeting, The Hague, Netherlands, June 26 - July 6, 1990.
2. A. Nadarajah, *Modelling the Solution Growth of TGS Crystals in Low Gravity*, Eighth American Conference on Crystal Growth, Vail, Colorado, July 15-21, 1990.

3. J.I.D. Alexander, *Commercial Numerical Codes: To Use or Not to Use, Is This The Question?*, Microgravity Fluids Workshop, Westlake Holiday Inn, Cleveland Ohio, August 7-9, 1990.
4. F. Rosenberger, *Fluid Transport in Materials Processin,* Microgravity Fluids Workshop, Westlake Holiday Inn, Cleveland Ohio, August 7-9, 1990.
5. F. Rosenberger, *Influence of Residual Gravity on Crystal Growth Processes*, First International Microgravity Congress, Bremen, September 1990 (invited).
6. J.I.D. Alexander, *Residual Acceleration Effects on Low Gravity Experiments*, Institute de Mechaniques des Fluides de Marseilles, Université de Aix-Marseille III, Marseille, France, January 1991, (3-lecture series, invited).
7. J.I.D. Alexander, *An Analysis of the Low Gravity Sensitivity of the Bridgman-Stockbarger Technique,* Department of Mechanical Engineering at Clarkson University, April 1991 (invited).
8. A. Nadarajah, *Measuring Diffusion Coefficients of Concentrated Solutions,* Fifth Annual Alabama Materials Research Conference, Birmingham September 1991.
9. A. Nadarajah, *Modelling Crystal Growth Under Low Gravity, Annual* Technical Meeting of the Society of Engineering Science, Gainesville, November 1991.
10. J.I.D. Alexander, *Vibrational Convection and Transport Under Low Gravity Conditions,* Society of Engineering Science 28th Annual Technical Meeting, Gainesville, Florida, November 6-7, 1991.
11. F. Rosenberger, *Theoretical Review of Crystal Growth in Space - Motivation and Results*, International Symposium on High Tech Materials, Nagoya, Japan, November 6-9, 1991 (plenary lecture, invited).
12. F. Rosenberger, *Computer Simulation in Materials Science*, Mitsubishi Frontiers Research Institute, Tokyo, Japan, November 8, 1991 (invited).
13. F. Rosenberger, *Importance of Materials Research in Space Laboratories for Industrial Development*, International Symposium for Promoting Applications and Capabilities of the Space Environment, Tokyo, Japan, November 14-15, 1991 (plenary lecture, invited).
14. F. Rosenberger, *What Can One Learn from 10 Second Low-Gravity Experiments?*, In Space 1991, Tokyo, Japan, November 14-15, 1991 (plenary lecture invited).
15. P. Larroude, J. Ouazzani and J.I.D. Alexander, *Flow Transitions in a 2D Directional Solidification Model,* 6th Materials Science Symposium, European Space Agency, Brussels, Belgium, 1992 (poster).
16. F. Rosenberger, *Microgravity Materials Processing and Fluid Transport*, AIAA Course on Low-Gravity Fluid Dynamics, AIAA Meeting, Reno, NV, January 10-12, 1992 (3-lecture series, invited).

17. J.I.D Alexander, *Numerical Simulation of Low-g Fluid Transport,* AIAA Course on Low-Gravity Fluid Mechanics, Reno, NV, January 10-12, 1992 (invited).
18. F. Rosenberger, *Time Scales in Transport Processes and Challenges for Short-Duration Low-Gravity Experiments*, Falltower Days Bremen, Bremen, Germany, June 1-3, 1992 (invited).
19. J.I.D. Alexander, *Modelling or Muddling? Analysis of Buoyancy Effects on Transport under Low Gravity Conditions,* World Space Congress, Washington, DC, August 28 - September 5, 1992 (invited lecture).

A CHEBYSHEV COLLOCATION METHOD FOR MOVING BOUNDARIES, HEAT TRANSFER, AND CONVECTION DURING DIRECTIONAL SOLIDIFICATION

Yiqiang Zhang, J. Iwan D. Alexander and Jalil Ouazzani*

Center for Micogravity and Materials Research, University of Alabama in Huntsville

Abstract

Free and Moving Boundary problems require the simultaneous solution of unknown field variables and the boundaries of the domains on which these variables are defined. There are many technologically important processes that lead to moving boundary problems associated with fluid surfaces and solid-fluid boundaries. These include crystal growth, metal alloy and glass solidification, melting and flame propagation. The directional solidification of semi-conductor crystals by the Bridgman-Stockbarger method[1,2] is a typical example of a such a complex process. A numerical model of this growth method must solve the appropriate heat mass and momentum transfer equations and detemine the location of the melt-solid interface. In this work, a Chebyshev pseudospectral collocation method is adapted to the problem of directional solidification. Implementation method involves a solution algorithm that combines domain decomposition, a finite-difference preconditioned conjugate minimum residual method and a Picard type iterative scheme.

---

* Presently at the Institute de Mécanique des Fluides de Marseille, 1 rue Honnorat, Marseille, France.

1. INTRODUCTION

Moving and free boundary problems are problems that require as part of the solution the determination of some or all the boundaries of the domain under consideration. Included in this class of problems are situations that involve fluid surfaces, or solid-fluid interfaces. Freezing and melting, crystal growth, flame propagation, liquid surface configurations, are examples of such processes that are important in a variety of areas with technological applications. Such problems generally pose a challenging problem to the numerical modeller. The Bridgman-Stockbarger directional solidification crystal growth technique is a typical example of such a complex problem. To adequately represent the physics of the problem, the solution method must be able to cope with the following: The unknown location of the crystal-melt interface, high Rayleigh number buoyancy-driven flows, heat transfer by conduction (along ampoule walls and in the crystal), convective-diffusive heat transfer in the melt and radiative and convective heat transfer between the furnace and the ampoule. Even for pure melts, due to differences in thermal conductivities between melt , crystal and ampoule, and the differences in thermal and momentum diffusivities in the melt, the problem has a variety of disparate length scales over which characteristic features must be accurately represented.

In past work[3-11], the Finite Element Method (FEM) has been successfully applied to the problem of computing melt and crystal temperature and concentration distributions, melt convection and the location of the crystal-melt interface. As an alternative to FEM we present a Chebyshev collocation(pseudospectral) method suitable for the solution of this class of problem. Spectral and pseudospectral methods[12-13] involve the representation of the solution as a truncated series of smooth functions of the independent variables. In contrast to FEM, for which the solution is approximated locally with expansions of local basis functions, spectral methods represent the solution as an expansion in global functions. In this sense they may be viewed as an extension of the separation of variables technique applied to complicated problems[14].

For problems that are characterized either by irregularly shaped domains, or even domains of unknown shape, it is, in general, neither efficient nor advantageous to try to find special sets of

spectral functions that are tuned to the particular geometry in consideration (especially in the case of solidification, where the melt-crystal geometry is not known *a priori*). Two alternative methods are mapping and patching[14]. Mapping allows an irregular region to be mapped into a regular one (which facilitates the use of known spectral functions, such as Chebyshev polynomials). For directional solidification systems (see Fig. 1) the melt-crystal boundary and, thus, the melt and crystal geometries, are unknown. Nevertheless, by specifying the melt-crystal boundary as some unknown single-valued function, the melt and crystal geometries can be mapped into simple ones by a smooth transformation. This mapping facilitates the use of Chebyshev polynomials to approximate the dependent variables in these new domains.

As can be seen from Figs. 1 and 2, heat transfer to and in the ampoule wall must also be considered. To do this we employ patching by subdividing the system into four domains (crystal, melt and two ampoule domains), and transform these domains to domains with simple shapes. We then solve the resulting problems in each domain and solve the full problem in the complicated domain by applying suitable continuity conditions across any boundaries (real or artificial) between the domains.

The formulation of the problem is outlined in section 2. The solution method is described in section 3. Our results are presented in section 4 and discussed in section 5.

2. FORMULATION

The vertical Bridgman-Stockbarger system is depicted in Fig. 2. A cylindrical ampoule with inner and outer diameters of $2R_0$ and $2(R_0+R_w)$ contains melt and crystal. To grow the crystal the ampoule must be translated relative to a prescribed external temperature gradient. The objective of this model is to describe a steady growth process that, in reality, can be achieved between initial and terminal transients in sufficiently long ampoules. Toward this end a pseudo-steady state model[2] is employed that neglects the ends of the ampoule. The remainder of the ampoule is assumed to occupy a cylindrical computational region of length L. Ampoule translation is then accounted for by supplying a melt to the top of the computational space at a uniform velocity, and withdrawing crystal from the bottom at the same velocity. It is thus assumed that there is no lag

between the translation rate and the crystal's growth velocity. Transport of heat from the furnace to the ampoule is modelled using a prescribed furnace temperature profile. The heat transfer from the furnace to the outer ampoule wall is governed by a heat transfer coefficient Bi(z). This is discussed in more detail later. The top and bottom of the ampoule are respectively assigned temperatures of T_H and T_C ($T_H > T_C$).

The variables are cast in dimensionless form by using R_0, α_L/R_0, $R_0\alpha_L$, α_L/R_o^2 and $T_H - T_C$, where α_L is the melt's thermal diffusivity, to scale length, velocity, stream function, vorticity and temperature, respectively. That is,

$$\mathbf{x} = (r,z)=(\tilde{r},\tilde{z})/R_0,\ \mathbf{u} = \tilde{\mathbf{u}}\, R_0/\alpha_L,\ \psi = \tilde{\psi}/\, R_0\alpha_L\ ,\ \omega = \tilde{\omega}R_0^2/\alpha_L,\ T = \frac{\tilde{T} - \tilde{T}_C}{\tilde{T}_H - \tilde{T}_C}\ . \qquad (1)$$

Here r and z represent the radial and axial coordinates, ψ is the stream function, ω is the vorticity and $\mathbf{u} = (u,w)$ represents velocity with radial and axial components u and w, respectively. A tilde denotes a dimensional quantity. Melt, crystal and ampoule temperatures will be distinguished by the suffixes L (melt), S (crystal)and W (ampoule) when necessary. The location of the crystal melt boundary is given by z=h(r,t) and must be determined. The melt is assumed to be incompressible and the stream function and vorticity are defined by the velocity components (u,w) as

$$u = \frac{1}{r}\frac{\partial\psi}{\partial z},\quad w = \frac{-1}{r}\frac{\partial\psi}{\partial r},\ \omega = \frac{\partial u}{\partial z} - \frac{\partial w}{\partial r}\ . \qquad (2)$$

The governing equations then take the following form

In the melt, $0 < r < 1$, $0 < z < h(r,z)$

$$u\frac{\partial\omega}{\partial r} + w\frac{\partial\omega}{\partial z} - \frac{\omega u}{r} = Pr\left(\frac{\partial^2\omega}{\partial r^2} + \frac{1}{r}\frac{\partial\omega}{\partial r} + \frac{\partial^2\omega}{\partial z^2}\right) - Pr\frac{\omega}{r^2} + Pr^2Gr\frac{\partial T}{\partial r}\ , \qquad (3)$$

$$r\omega = \frac{\partial^2\psi}{\partial r^2} - \frac{1}{r}\frac{\partial\psi}{\partial r} + \frac{\partial^2\psi}{\partial z^2}\ , \qquad (4)$$

and

$$u\frac{\partial T}{\partial r} + w\frac{\partial T}{\partial z} = \Delta T \quad , \quad \Delta = \frac{\partial^2}{\partial r^2} + \frac{1}{r}\frac{\partial}{\partial r} + \frac{\partial^2}{\partial z^2}, \tag{5}$$

where $Pr = \nu/\alpha_L$ is the Prandtl number, $Gr = \beta(T_H - T_C)gR_0^3/\nu^2$ is the Grashof number, ν is the melt's viscosity and β is the melt's thermal expansion coefficient.

In the crystal, $0 < r < 1$, $h(r) << z < \Lambda$,

$$\alpha' Pe\frac{\partial T}{\partial z} = \Delta T, \tag{6}$$

and in the ampoule wall, $1 < r < r_w$, $0 < z < \Lambda$,

$$\alpha'' Pe\frac{\partial T}{\partial z} = \Delta T, \tag{7}$$

where α', and α'' are, respectively, the ratios of the melt's thermal diffusivity with the crystal and ampoule thermal diffusivities, and $Pe = V_0R_0/\alpha_L$ is the Peclet number and V_0 is the ampoule translation rate.

For the temperature the boundary conditions are:

At the melt-crystal interface $z = h(r,t)$

$$T_L = T_S = T_M, \tag{8}$$

$$k'\nabla T_L\mathbf{n} - \nabla T_S\mathbf{n} = StPe\,\alpha'\mathbf{n}\cdot\mathbf{e}_z, \tag{9}$$

where T_M represents the dimensionless melting temperature, k' is the ratio of melt and crystal conductivities, $St = \Delta H/(C_{ps}\Delta T)$ is the Stefan number. The vector $\mathbf{n}$ is the unit normal to the crystal-melt surface and points into the melt. At the outer ampoule wall, $r = r_w$

$$-\frac{\partial T}{\partial r} = Bi(z)(T - T_F(z)). \tag{10}$$

The temperatures at $z=0$ and $z=\Lambda$ are constant, i.e.

$$T(r,0) = 1,\ T(r,\Lambda) = 0, \tag{11}$$

and the heat flux is continuous across the inner ampoule wall

$$\left(\frac{\partial T(1,z)}{\partial r}\right)_L = k^*\left(\frac{\partial T(1,z)}{\partial r}\right)_W$$
$$\left(\frac{\partial T(1,z)}{\partial r}\right)_S = k^{**}\left(\frac{\partial T(1,z)}{\partial r}\right)_W \qquad (12)$$

In (10) Bi(z) is a heat transfer coeffcient and $T_F(z)$ is the furnace temperature profile. The coefficients k* and k** represent the ratio of the wall conductivity with that of the melt and ampoule, respectively.

For the stream function the boundary conditions are

$$\psi(0,z) = 0,\ \psi(1,z) = -\frac{1}{2}Pe,\ \psi(0,z) = -\frac{1}{2}r^2Pe,\ \psi(h(r),z) = -\frac{1}{2}r^2Pe, \qquad (13)$$

and the vorticity is zero at r=0. At the other melt boundaries the boundary conditions for the vorticity are enforced (iteratively) using previously computed values of the velocity field (the scheme is explained in section 3.3. The velocity boundary conditions are

$$u(0, z) = u(1,z)=u(r,h(r)) =0;\ w(0,z) = w(1,z)= w(r,h(r))=Pe. \qquad (14)$$

Note that, at the melt-crystal boundary there are two boundary conditions for the temperature. In the following section we describe an iterative scheme which distinguishes one of the temperature boundary conditions and uses it to compute the interface shape iteratively.

3. SOLUTION METHOD

The solution method is based on a Picard[15] type iteration which consists essentially of four steps:

1. The initial shape of the crystal-melt interface is specified and an independent variable transformation is applied to the governing equations and boundary conditions in the melt, crystal an ampoule regions. This specifies the computational domains.

2. The coupled momentum, heat, mass and species equations are then solved using three of the four boundary conditions on the moving boundary.

3. The remaining boundary condition (or *distinguished* condition[2]), in this case equation (8), is used to compute corrected boundary locations.

4. Steps 2 and 3 are repeated until the distinguished boundary condition is satisfied.

The solution method is implemented using domain decomposition and a preconditioned generalized conjugate residual method[13,16]

3.1 Domain Decomposition

The physical region is split into four computational domains, Ω_i, i=1,...,4. The domains correspond to the melt (Ξ_1), the crystal (Ξ_3), and the portions of the ampoule wall adjacent to the melt (Ξ_2) and the crystal (Ξ_4). The irregularly shaped domains are mapped onto rectangular regions by

$$\xi = r, \eta = \frac{z}{h(r)}, \Xi_1 \rightarrow \Omega_1, \tag{15}$$

$$\xi = r, \eta = \frac{z}{h(1)}, \Xi_2 \rightarrow \Omega_2, \tag{16}$$

$$\xi = r, \eta = 2 - \frac{z - \Lambda}{h(r) - \Lambda}, \Xi_3 \rightarrow \Omega_3 . \tag{17}$$

$$\xi = r, \eta = 2 - \frac{z - \Lambda}{h(1) - \Lambda}, \Xi_4 \rightarrow \Omega_4 . \tag{18}$$

3.2 Spatial discretization

The dependent variables, Φ are approximated by Chebyshev polynomials[12,13], i.e

$$\Phi = \Phi_{NM}(X_i, Y_j) = \sum_{\substack{i=0 \\ j=0}}^{N,M} a_{ij} T_{ij}(X_i, Y_j), \tag{19}$$

where $T_{ij} = T_i T_j$, and the T_k are Chebyshev polynomials of order k. The points (X_i , Y_j) are related to the coordinates ξ and η by

$$\xi = aX + b, \eta = cY + d, \tag{20}$$

where a and b are determined by the transformation of each domain, Ω_i, to [-1,1]×[−1,1]. The discrete points (X_i,Y_j), i=0, N, j=0,M,are the Gauss-Lobatto collocation points[13]. That is,

$$X_i = \cos \pi \left[\frac{i}{N}\right], i = 0, 1, ..., N \tag{21}$$

$$X_i = \cos \pi \left[\frac{i}{N}\right], i = 0, 1, ..., N, \tag{22}$$

The spatial derivatives are given by

$$\frac{\partial \Phi}{\partial \xi} = \frac{1}{a}\frac{\partial \Phi}{\partial X}, \frac{\partial \Phi}{\partial \eta} = \frac{1}{c}\frac{\partial \Phi}{\partial Y}, \frac{\partial^2 \Phi}{\partial \xi \partial \eta} = \frac{1}{ac}\frac{\partial^2 \Phi}{\partial X \partial Y}, \frac{\partial^2 \Phi}{\partial \xi^2} = \frac{1}{a^2}\frac{\partial^2 \Phi}{\partial X^2}, \frac{\partial^2 \Phi}{\partial \eta^2} = \frac{1}{c^2}\frac{\partial^2 \Phi}{\partial Y^2} \tag{23}$$

where the derivatives with respect to X and Y have the forms

$$\frac{\partial \Phi(X, Y)}{\partial X} \approx \frac{\partial \Phi(X_i, Y_j),}{\partial X} = \sum_{p=0}^{N} D_x^{ip} \Phi(X_p, Y_j) = \sum_{p=0}^{N} D_x^{ip} \Phi \, pj, \tag{24}$$

$$\frac{\partial \Phi(X, Y)}{\partial Y} \approx \frac{\partial \Phi(X_i, Y_j),}{\partial Y} = \sum_{q=0}^{N} D_x^{jq} \Phi(X_i, Y_q) = \sum_{q=0}^{N} D_x^{jq} \Phi \, iq, \tag{25}$$

$$\frac{\partial^2 \Phi(X, Y)}{\partial X^2} \approx \frac{\partial \Phi(X_i, Y_j),}{\partial X^2} = \sum_{p=0}^{N} D_{xx}^{ip} \Phi(X_p, Y_j) = \sum_{p=0}^{N} D_x^{ip} \Phi \, pj, \tag{26}$$

$$\frac{\partial^2 \Phi(X, Y)}{\partial Y^2} \approx \frac{\partial^2 \Phi_{NM}(X_i, Y_j),}{\partial Y^2} = \sum_{q=0}^{M} D_{yy}^{iq} \Phi(X_i, Y_q) = \sum_{q=0}^{M} D_{yy}^{iq} \Phi \, iq, \tag{27}$$

$$\frac{\partial^2 \Phi(X_i, Y_j)}{\partial XY} = \sum_{\substack{p=0 \\ q=0}}^{N, M} D_x^{ip} D_y^{jq} \Phi(X_p, Y_q) = \sum_{\substack{p=0 \\ q=0}}^{N, M} D_x^{ip} D_y^{jq} \Phi_{pq}, \tag{28}$$

where the expressions for $\mathbf{D_x}$, $\mathbf{D_y}$, $\mathbf{D_{xx}}$, $\mathbf{D_{yy}}$ and $\mathbf{D_{xy}}$ are given explicitly by Ouazzani[17].

3.3 Pseudo-unsteady discretization

The governing equations now have the form

$$(A^{(i)} - \Delta^{(i)})\phi^{(i)} = S^{(i)},\ i = 1,6 \tag{29}$$

where the $A^{(i)}$, $\Delta^{(i)}$, $S^{(i)}$ and $\phi^{(i)}$ are given in Appendix I. To solve these equations using a pseoudo- unsteady iterative scheme (28) is rewritten as

$$(\frac{\partial \phi^{(i)}}{\partial \tau} + A^{(i)})\phi^{(i)} = S^{(i)} + \Delta^{(i)}\phi^{(i)},\ i = 1,6 \tag{30}$$

The left-hand side of (29) is written in discrete form as

$$(\frac{\partial \phi}{\partial \tau} + A)\phi = (A + \sigma I)\phi^{n+1} - \sigma\phi^{n}, \tag{31}$$

where $\sigma^{(i)} = 1/\Delta\tau^{(i)}$ for i=1,2,4,5,6 and is zero for i=3. the index in parentheses has been omitted for clarity and the superscript denotes the pseudo-time or iterative step number. Note that the time step size, $\Delta\tau^{(i)}$, is generally different for each of the equations.

The problem now has the form

$$\mathbf{H}_{sp}\phi^{n+1} + \sigma\mathbf{I}\phi^{n+1} = \mathbf{F}(\phi,h)^{n}, \tag{32}$$

where

$$\mathbf{H}_{sp} = A - \Delta, \quad \text{and} \quad \mathbf{F} = S + \sigma\phi^{n}, \tag{33}$$

and $\mathbf{H}_{sp}$ is obtained from the expressions in Appendix B using the Chebyshev derivatives (26)-(28) and equation (23). A superscript n denotes a quantity evaluated at the nth iterative step (note that the indices in parethenses have been omitted for clarity) .

3.4 Vorticity boundary condition

To solve the vorticity-stream function equations we adopted the following procedure which is simply an extension, for Chebyshev approximations, of an approach described by Peyret [12]. The velocity field is calculated from the stream function obtained from the previous iteration. The vorticity at the boundary which corresponds to this velocity field is then found from

$$\hat{\omega}^{n+1} = \left(\frac{\partial u}{\partial z} - \frac{\partial w}{\partial r}\right)^{n}, \tag{34}$$

and the value of the vorticity to be applied at the boundary, ω^{n+1}, is given by

$$\omega^{n+1} = \gamma\hat{\omega}^{n+1} + (1-\gamma)\omega^{n}. \tag{35}$$

Here γ $(0 < \gamma < 1)$ is a relaxation parameter.

3.5 Preconditioned Generalized Conjugate Residual Method

The operator $\mathbf{H}_{sp}$ is represented by a full matrix of order $(N+1)^2 \times (M+1)^2$ and is not symmetric. In order to solve the system of equations and boundary conditions represented by (28)-(32) and (A.9)-(A.18), each of the spectral operators $\mathbf{H}_{sp}$ for each of the domains Ω_i , i=1,4 and the conditions on shared domain boundaries $\Omega_i \cap \Omega_i$, $i \neq j$, i,j=1,4 are combined and approximated by a single finite difference operator $\mathbf{H}_{fd}$. This is defined over the entire domain $\Omega = \bigcup_{i=1}^{4} \Omega_i$. The following iterative procedure which consisits of inner and outer loops is then adopted:

Outer loop: First an initial interface shape h^0 is assumed

Inner loop: The residual $\mathbf{R}$ is then initialized by

$$\mathbf{R}^0 = \mathbf{H}_{sp}^{*}\Phi - \mathbf{F}, \tag{36}$$

where Φ represents the $\phi^{(i)}$. Then we solve

$$\mathbf{H}_{fd}^{*}\Theta^0 = \mathbf{R}^0, \tag{37}$$

where $\mathbf{H}^{*} = \mathbf{H} + \sigma\mathbf{I}$. Then we set

$$\mathbf{P}^0 = \Theta^0, \tag{38}$$

and calculate

$$\alpha_{m+1} = \frac{(\mathbf{R}^m, \mathbf{H}_{sp}\mathbf{P}^m)}{(\mathbf{H}_{sp}\mathbf{P}^m, \mathbf{H}_{sp}\mathbf{P}^m)}. \tag{39}$$

The variables Φ are then updated from

$$\Phi^{m+1} = \Phi^m + \alpha_{m+1}\mathbf{P}^m, \tag{40}$$

and the problem

$$\mathbf{H}^*_{fd}\Theta^{m+1} = \mathbf{R}^{m+1}, \tag{41}$$

is solved for Θ. $\mathbf{P}$ is then updated using

$$\mathbf{P}^{m+1} = \Theta^m + \sum_{j=0}^{\infty} \beta_j^{m+1}\mathbf{P}^j, \tag{42}$$

where

$$\beta_j^{m+1} = \frac{(\mathbf{H}_{sp}\Theta^{m+1}, \mathbf{H}_{sp}\mathbf{P}^j)}{(\mathbf{H}_{sp}\mathbf{P}^j, \mathbf{H}_{sp}\mathbf{P}^j)}. \tag{43}$$

The procedure is continued until $|\mathbf{R}| < \varepsilon$.

The preconditioned problem is given by equations (37) and (41). The finite difference operator $\mathbf{H}^*_{fd}$ is approximated by incomplete LU decomposition. The solution for Θ is obtained by forward and backward substitution. The subsequent approximations to $\Phi = (T_S, T_L, \omega, \psi)$ are then obtained from (40). At this point we note that while we used a nine-diagonal matrix for the second-order central finite difference operator for the solution of the temperature field, a seven diagonal operator was used for the solution of the stream-function and vorticity as it appeared to lead to more rapid convergence. This means that the cross-derivative terms were evaluated at the previous time step and were included in $\mathbf{F}$ on the right-hand side of (32).

3.6 Interface Shape Update

This iterative procedure is repeated until the convergence criterion is satsified. The first of equations (A.17) is used as a distinguished boundary condition. If it is not satisfied, another outer loop iteration is performed and the interface shape is relocated using either Newton's method

$$h_i^{n+1} = h_i^n + \left(\frac{\partial\theta}{\partial h}\right)_i^{-1} \theta_i \tag{44}$$

where θ_i is the difference between the temperature at the ith interfacial site and the melting temperature T_m; or from a searching method

$$h_i^{n+1} = h_i^n + \alpha(T_i - T_M). \tag{45}$$

Here α is found by numerical experiment. We found that by using the Newton method for the first few iterations and then the searching method for subsequent iterations, we achieved better success than with the Newton method alone.

4. RESULTS

We carried out several tests of the method. The results are shown in Table 1 and in Figs. 3 and 4. The parameters used are given in Appendix C and correspond to the thermophysical properties of Gallium-doped Germanium. For the cases examined our results are in good agreement with the FEM calculations of Adornato and Brown.[2] For example, the difference between our results and theirs for the maximum stream function computed for Fig. 3c is less than 2%.

Figure 2 shows results for a furnace with a constant temperature gradient and Bi=7.143. That is,

$$T_f(z) = 1 - z\Lambda^{-1}. \tag{46}$$

The isotherms are practically flat except at the crystal-melt boundary where the mismatch in thermal conductivity results in a convex interface. The flow depicted by the streamlines in Fig. 3b-d is a

combination of the ampoule translation (which, if buoyant convection were absent, would appear as a set of vertical streamlines parallel to the ampoule wall) and buoyant flow caused by radial gradients in temperature. This results in an upward flow of hot melt near the ampoule wall and a downflow near the ampoule centerline. Note the increase in flow intensity as the Grashof number is increased.

Figure 4 shows results for different Grashof numbers for a non-uniform furnace temperature

profile

$$T_f(z) = 0.5[1 + \tanh(6 - 12z\Lambda^{-1})] \tag{47}$$

together with a position dependent heat transfer function given by

$$Bi(z) = 0.2\{2[1 + \tanh(5 - 2z)] + 1 + \tanh(2z - 15)\}. \tag{48}$$

Radial temperature gradients arise for two reasons in this problem: The mismatch in thermal conductivities at the ampoule-melt-crystal junction and the change in heat transfer at the quasi-adiabatic zones. These zones are created by the furnace temperature profile and conditions (47) and (48). This heating configuration produces two counter rotating cells. The upper cell increases in spatial extent as the Grashof number is increased.

Table 1 shows the CPU times, number of iterations taken to converge and compiler options for the case shown in Fig. 4b for a CRAY/XMP, an iPSC parallel processor and an Ardent Titan computer.

5. DISCUSSION

Chebyshev spectral methods that have been shown to achieve superior accuracy for a wide range of fluid flow problems defined in regular geometries can be applied to problems involving unknown free and moving irregular boundaries through a combination of mapping and domain decomposition. For the directional solidification described here, this was achieved without incurring excessive CPU times and has been implemented on several different machines to illustrate the magnitude of the CPU times involved for a typical calculation. Whether there is

ultimately any advantage in using such spectral methods over finite elements will depend on the specific application. It will most likely depend on the accuracy required and on whether the ability of the Chebyshev collocation method to achieve better accuracy for a given number of collocation points (which is recognized for a variety of flows in regular geometries) is retained or degraded when using domain decomposition.

Acknowledgements

This work was supported by grant NAG8-790 from the National Aeronuatics and Space Administration, and by the State of Alabama through Albama Supercomputer Network and the Center for Microgravity and Materials Research at the University of Alabama in Huntsville. The authors would also like to thank Professors F. Rosenberger and R. Peyret for helpful comments and discussion.

Appendix A

Transformed Equations

After the equations and boundary conditions (2) - (14) have been transformed according to (15)-(18) we obtain the following equations.

For $0 < \eta < 1$

$0 < \xi < 1$

$$\frac{1}{\xi h}\left(\frac{\partial T}{\partial \xi}\frac{\partial \psi}{\partial \eta} - \frac{\partial T}{\partial \eta}\frac{\partial \psi}{\partial \xi}\right) = \Delta^* T\,, \tag{A.1}$$

$$\frac{1}{\xi h}\left(\frac{\partial \psi}{\partial \eta}\frac{\partial \omega}{\partial \xi} - \frac{\partial \psi}{\partial \xi}\frac{\partial \omega}{\partial \eta} - \frac{\omega}{\xi}\frac{\partial \psi}{\partial \eta}\right) = Pr\Delta^*\omega - Pr\frac{\omega}{\xi^2} + Pr^2 Gr\left(\frac{\partial T}{\partial \xi} - \frac{\eta}{h}\frac{dh}{dr}\frac{\partial T}{\partial \eta}\right), \tag{A.2}$$

$$\frac{\partial^2 \psi}{\partial \xi^2} + A\frac{\partial^2 \psi}{\partial \eta^2} + B\frac{\partial^2 \psi}{\partial \xi \partial \eta} - \frac{1}{\xi}\frac{\partial \psi}{\partial \xi} + C\frac{\partial \psi}{\partial \eta} = \xi\omega, \tag{A.3}$$

where

$$\Delta^* = \frac{\partial^2}{\partial \xi^2} + A\frac{\partial^2}{\partial \eta^2} + B\frac{\partial^2}{\partial \xi \partial \eta} + \frac{1}{\xi}\frac{\partial}{\partial \xi} + C\frac{\partial}{\partial \eta}\,, \tag{A.4}$$

and

$$A=\frac{1}{h^2}+\left(\frac{\eta}{h}\frac{dh}{dr}\right)^2,\ B=\frac{-2\eta}{h}\frac{dh}{dr},\ C=\eta\left[2\left(\frac{1}{h}\frac{dh}{dr}\right)^2-\frac{1}{h}\frac{d^2h}{dr^2}-\frac{1}{\xi h}\frac{dh}{dr}\right]. \tag{A.5}$$

For $1<\eta<2$

$0<\xi<1$

$$\Delta^{**}T-\mathrm{Pe}\,\alpha'\frac{1}{h}\frac{\partial T}{\partial\eta}=0, \tag{A.6}$$

where

$$\Delta^{**}=\frac{\partial^2}{\partial\xi^2}+A^*\frac{\partial^2}{\partial\eta^2}+B^*\frac{\partial^2}{\partial\xi\partial\eta}+\frac{1}{\xi}\frac{\partial}{\partial\xi}+C^*\frac{\partial}{\partial\eta}, \tag{A.7}$$

and

$$A^*=\frac{1}{(h-\Lambda)^2}+\left(\frac{\eta-2}{h-\Lambda}\frac{dh}{dr}\right)^2,\ B^*=\frac{-2}{h-\Lambda}(\eta-2)\frac{dh}{dr},$$

$$C^*=(\eta-2)\left[2\left(\frac{1}{h-\Lambda}\frac{dh}{dr}\right)^2-\frac{1}{h-\Lambda}\frac{d^2h}{dr^2}-\frac{1}{\xi(h-\Lambda)}\frac{dh}{dr}\right]. \tag{A.8}$$

In the ampoule wall, $1<\xi<r_w$, $0<\eta<2$, where h(r) is taken to be a constant at each inner iteration, we have

$$\frac{\partial^2T}{\partial\xi^2}+\frac{1}{h^2}\frac{\partial^2T}{\partial\eta^2}+\frac{1}{\xi}\frac{\partial T}{\partial\xi}-\mathrm{Pe}\,\alpha''\frac{1}{h}\frac{\partial T}{\partial\eta}=0,\ 0<\eta<1, \tag{A.9}$$

and

$$\frac{\partial^2T}{\partial\xi^2}+\frac{1}{(h-\Lambda)^2}\frac{\partial^2T}{\partial\eta^2}+\frac{1}{\xi}\frac{\partial T}{\partial\xi}+\mathrm{Pe}\,\alpha''\frac{1}{h-\Lambda}\frac{\partial T}{\partial\eta}=0,\ 1<\eta<2. \tag{A.10}$$

The boundary conditions become

$$\frac{\partial T}{\partial\xi}=0,\ \psi=0,\ \omega=0\ \text{at}\ \xi=0, \tag{A.11}$$

$$T=1,\ \psi=-1/2\xi^2\mathrm{Pe},\ \text{at}\ \eta=0, \tag{A.12}$$

$$\psi = -\frac{1}{2}\mathrm{Pe},$$

$$\left(\frac{\partial T_L}{\partial \xi} - \frac{\eta}{h}\frac{dh}{dr}\frac{\partial T_L}{\partial \eta}\right) = k^{*}\frac{\partial Tw}{\partial \xi} \text{ at } \xi = 1,\ 0 < \eta < 1, \tag{A.13}$$

$$\left(\frac{\partial T_S}{\partial \xi} - \frac{\eta}{h-\Lambda}\frac{dh}{dr}\frac{\partial T_S}{\partial \eta}\right) = k^{**}\frac{\partial Tw}{\partial \xi},\ \ \xi = 1,\ 1 < \eta < 2 \quad , \tag{A.14}$$

$$\frac{\partial T}{\partial \xi} = \mathrm{Bi}(\eta)(T - T_F(\eta)),\ \ \xi = r_w,\ 0 < \eta < 2 \quad , \tag{A.15}$$

$$T = 0 \text{ at } \eta = 2,\ 0 < \xi < r_w \quad . \tag{A.16}$$

Finally, at the crystal melt interface the boundary conditions are

$$T = T_M,\ \frac{1}{h}k'\frac{\partial T_L}{\partial \eta} + \frac{1}{h-\Lambda}\frac{\partial T_S}{\partial \eta} = \frac{\mathrm{StPe}\alpha'}{1+\left(\frac{dh}{dr}\right)^2}, \tag{A.17}$$

and

$$\psi = -\frac{1}{2}\xi^2\mathrm{Pe},\ \text{at}\ \eta = 1,\ 0 < \xi < 1\ . \tag{A.18}$$

In (A.17) we have used the fact that the melting temperature T_M is assumed to be constant along the crystal melt interface (i.e. $\partial T/\partial \xi = 0$). The vorticity boundary condition is given by equation (35) with

$$\hat{\omega} = \frac{1}{h}\frac{\partial u}{\partial \eta} + \frac{\eta}{h}\frac{dh}{dr}\frac{\partial w}{\partial \eta} - \frac{\partial w}{\partial \xi}. \tag{A.19}$$

Appendix B

The $A^{(i)}$, $\Delta^{(i)}$ and $F^{(i)}$ referred to in section 3.3 are expressed in terms of the equations given in Appendix I as follows:

$\phi^{(1)} = T^{n+1}$

$$A^{(1)} = \frac{1}{\xi h}\left(\frac{\partial T^{n+1}}{\partial \xi}\frac{\partial \psi^n}{\partial \eta} - \frac{\partial T^{n+1}}{\partial \eta}\frac{\partial \psi^n}{\partial \xi}\right) \tag{B.1}$$

$$\Delta^{(1)} = \Delta^{*} \tag{B.2}$$

$$F^{(1)} = \sigma^{(1)}T^n \tag{B.3}$$

$\phi^{(2)} = \omega^{n+1}$

$$A^{(2)} = \frac{1}{\xi h}\left(\frac{\partial\psi^n}{\partial\eta}\frac{\partial\omega^{n+1}}{\partial\xi} - \frac{\partial\psi^n}{\partial\xi}\frac{\partial\omega^{n+1}}{\partial\eta} - \frac{\omega^{n+1}}{\xi}\frac{\partial\psi^n}{\partial\eta}\right) \tag{B.4}$$

$$\Delta^{(2)} = \Delta^* - \frac{Pr}{\xi^2} \tag{B.5}$$

$$F^{(2)} = Pr^2 Gr\left(\frac{\partial T^{n+1}}{\partial\xi} - \frac{\eta}{h}\frac{dh}{dr}\frac{\partial T^{n+1}}{\partial\eta}\right) + \sigma^{(2)}\omega^n \tag{B.6}$$

$\phi^{(3)} = \psi^{n+1}$

$$A^{(3)} = 0 \tag{B.7}$$

$$\Delta^{(3)} = \Delta^* - \frac{2}{\xi}\frac{\partial}{\partial\xi}, \tag{B.8}$$

$$F^{(3)} = \xi\omega^{n+1}, \tag{B.9}$$

$\phi^{(4)} = T_w{}^{n+1}$ $(0 < \eta < 1)$, $\phi^{(5)} = T_w{}^{n+1}$ $(1 < \eta < 2)$, $\phi^{(6)} = T_s{}^{n+1}$,

$$A^{(4)} = A^{(5)} = A^{(6)} = 0 \tag{B.10}$$

$$\Delta^{(4)} = \frac{\partial^2}{\partial\xi^2} + \frac{1}{h^2}\frac{\partial^2}{\partial\eta^2} + \frac{1}{\xi}\frac{\partial}{\partial\xi} - Pe\,\alpha''\frac{1}{h}\frac{\partial}{\partial\eta} \tag{B.11}$$

$$\Delta^{(5)} = \frac{\partial^2}{\partial\xi^2} + \frac{1}{(h-\Lambda)^2}\frac{\partial^2}{\partial\eta^2} + \frac{1}{\xi}\frac{\partial}{\partial\xi} + Pe\,\alpha''\frac{1}{h-\Lambda}\frac{\partial}{\partial\eta} \tag{B.12}$$

$$\Delta^{(6)} = \Delta^{**} - Pe\,\alpha'\frac{1}{h}\frac{\partial}{\partial\eta}, \tag{B.13}$$

$$F^{(i)} = \sigma^{(1)}\phi^{(i)},\ i = 4,5,6 \tag{B.14}$$

Appendix C

Physical constants, system dimensions and thermophysical properties of Gallium doped Germanium used in the calculations

Property	dimension	Ge:Ga
Growth velocity	[cms^{-1}]	4×10^{-4}
Ampoule length (L)	[cm]	
Constant gradient furnace (Fig. 2)		7.0
Heat pipe furnace (Fig. 3)		7.62
Outer ampoule radius (R_w)	[cm]	
Constant gradient furnace		0.7
Heat pipe furnace		0.952
Inner ampoule radius (R_0)		
Constant gradient furnace		0.5
Heat pipe furnace		0.762
Kinematic viscosity (ν)	[$cm^2\ s^{-1}$]	$1.3(10)^{-3}$
Thermal conductivity (ampoule)	[$W\ K^{-1}cm^{-1}$]	
Constant gradient furnace		3.27
Heat pipe furnace		0.26
Thermal conductivity (crystal)	[$W\ K^{-1}cm^{-1}$]	0.17
Thermal conductivity (melt)	[$W\ K^{-1}cm^{-1}$]	0.39
Density (crystal)	[$g\ cm^{-3}$]	5.5
Density (melt)	[$g\ cm^{-3}$]	5.5
Heat of solidification (ΔH)	[$J\ g^{-1}$]	460
Specific heat (melt)	$J\ K^{-1}g^{-1}$	0.39
Specific heat (crystal)	$J\ K^{-1}g^{-1}$	0.39
Thermal expansion coefficient	[K^{-1}]	$5\ (10)^{-4}$

References

1. B. Chalmers, *Principles of Solidification*, (Kreiger, Huntington, New York, 1964) .
2. R.K. Willardson and A.C. Beer, eds. *Semiconductors and Semimetals, Vol. 18*, (Academic Press, New York, 1981).

3. H. H. Ettouney and R. A. Brown, "Finite element methods for steady solidification problems", *J. Computational Physics* 49 (1983) 118.

4. C. Chang and R.A. Brown, "Finite element calculation of buoyancy-driven convection near al melt/solid boundary", *J. Computational Physics* **53**, 1-27, (1984).

5. C. J. Chang and R.A. Brown, "Radial segregation induced by natural convection and melt solid interface shape in vertical Bridgman growth", *J. Crystal Growth*, **63**, 343-364, (1983)

6. P. M. Adornato and R. A. Brown, "Convection and segregation in directional solidification of dilute and non-dilute binary alloys", *J. Crystal Growth*, **80**, 155-190 (1987).

7. P.M. Adornato and R.A. Brown, "Petrov-Galerkin methods for natural convection in directional solidification of non-dilute binary alloys", *Int. J. Num. Meth. Fluids*, **7**, 761-791 (1987).

8. D.H. Kim, P.M. Adornato and R.A. Brown, "Effect of vertical magnetic field on convection and segregation", *J. Crystal Growth* , **89**, 339-356 (1988).

9. C.J. Chang, B. Baird, P.-K. Liao, R. Chang and L. Colombo, Finite Element analysis on the crystal growth of HgCdTe", *J. Crystal Growth* , **98**, 595-609 (1989).

10. S. Brandon and J.J. Derby, Heat transfer in vertical Bridgman growth of oxides: effects of conduction, convection and internal radiation", *J. Crystal Growth*, **121**, 473-194 (1992).

11. D.H. Kim and R.A. Brown, "Models for convection and segregation in the growth of HgCdTe by the vertical Bridgman method", *J. Crystal Growth*, **96**, 609-627 (1989).

12. R. Peyret and T.D. Taylor, *Computational Methods for Fluid Flow* (Springer-Verlag, New York, 1983).

13. C. Canuto, M. Y. Hussaini, A. Quarteroni and T.A. Zang, *Spectral Methods in Fluid Dynamics* (Springer-Verlag, Berlin, 1988).

14. S. Orszag, "Spectral Methods for Problems in Complex Geometries",*J. of Computational Physics*, **37**, 70-92 (1980) .

15. J.M. Floryan, "Numerical Methods for Viscous Flows with Moving Boundaries", *Appl. Mech. Rev.* **42** 323-341 (1989).

16. Y.S. Wong, T.A. Zang, M.Y. Hussaini, "Preconditioned conjugate residual methods for the solution of spectral equations", *Computers and Fluids* **14**, 85-95 (1986).

17. J. Ouazzani, *Méthode Pseudo-Spectrale pour la Resolution des Équations d'un Melange de Gaz Binaire*, Thèse, Universitie of Nice (1984).

Figure Captions

Fig. 1 Typical Bridgman-Stockbarger set-up

Fig. 2 a) The model Bridgman-Stockbarger system and b) the computational domains

Fig.3 Results for results for a furnace with a constant temperature gradient, Bi=7.143 and a Pr = 0.07 melt, a) Gr = 5206, b) Gr = 52,060 c) Gr = 520,600

Fig. 4 Results for a non-uniform furnace temperature profile (47) and position dependent heat transfer coefficient (48) for Pr =0.007 and a) Gr = 7,140, b) Gr = 14280 c) Gr=71,400 d) Gr= 142,800 .

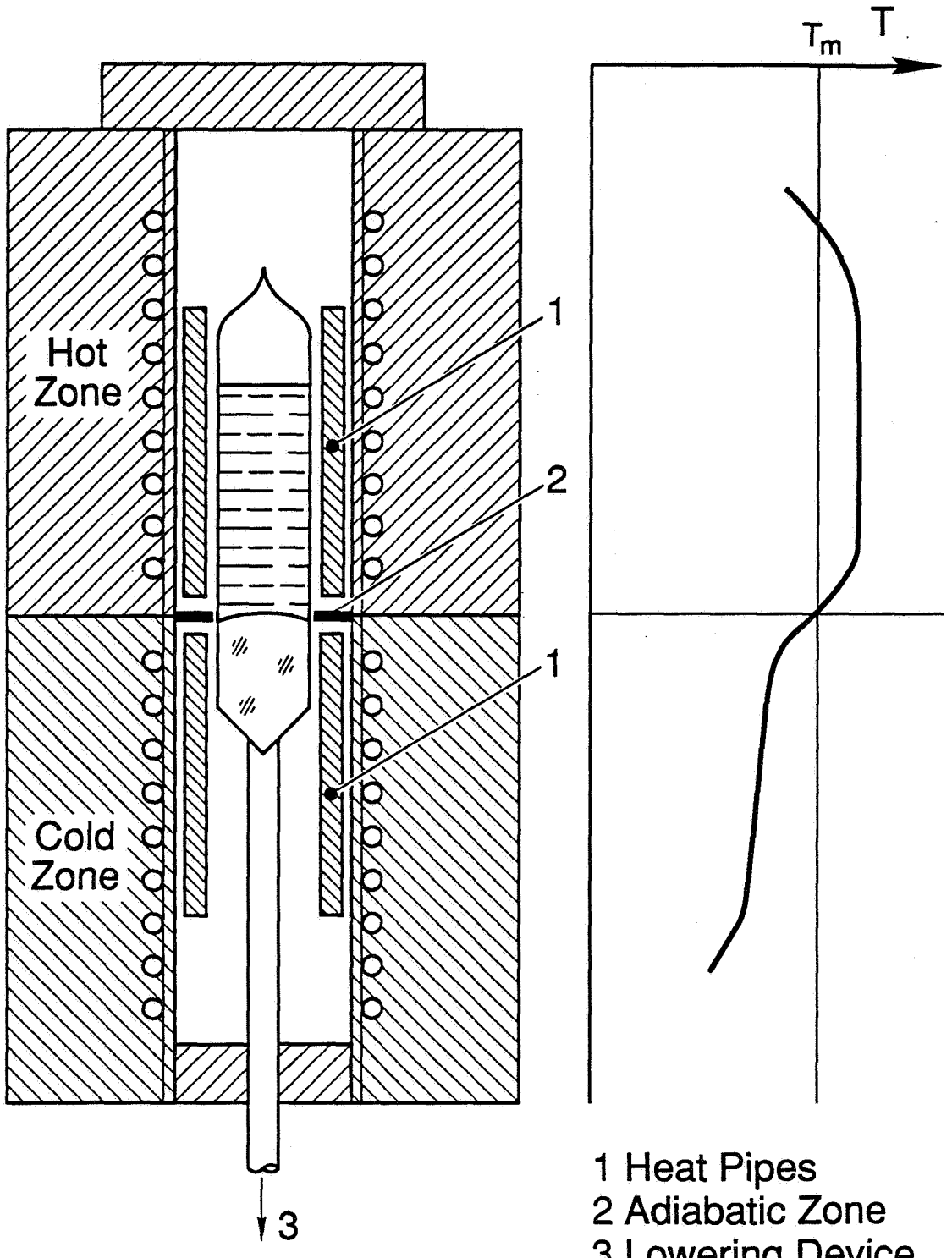
Hot
Zone
Cold
Zone
1
2
1
3
T_m
T
1 Heat Pipes
2 Adiabatic Zone
3 Lowering Device

FIG. 1

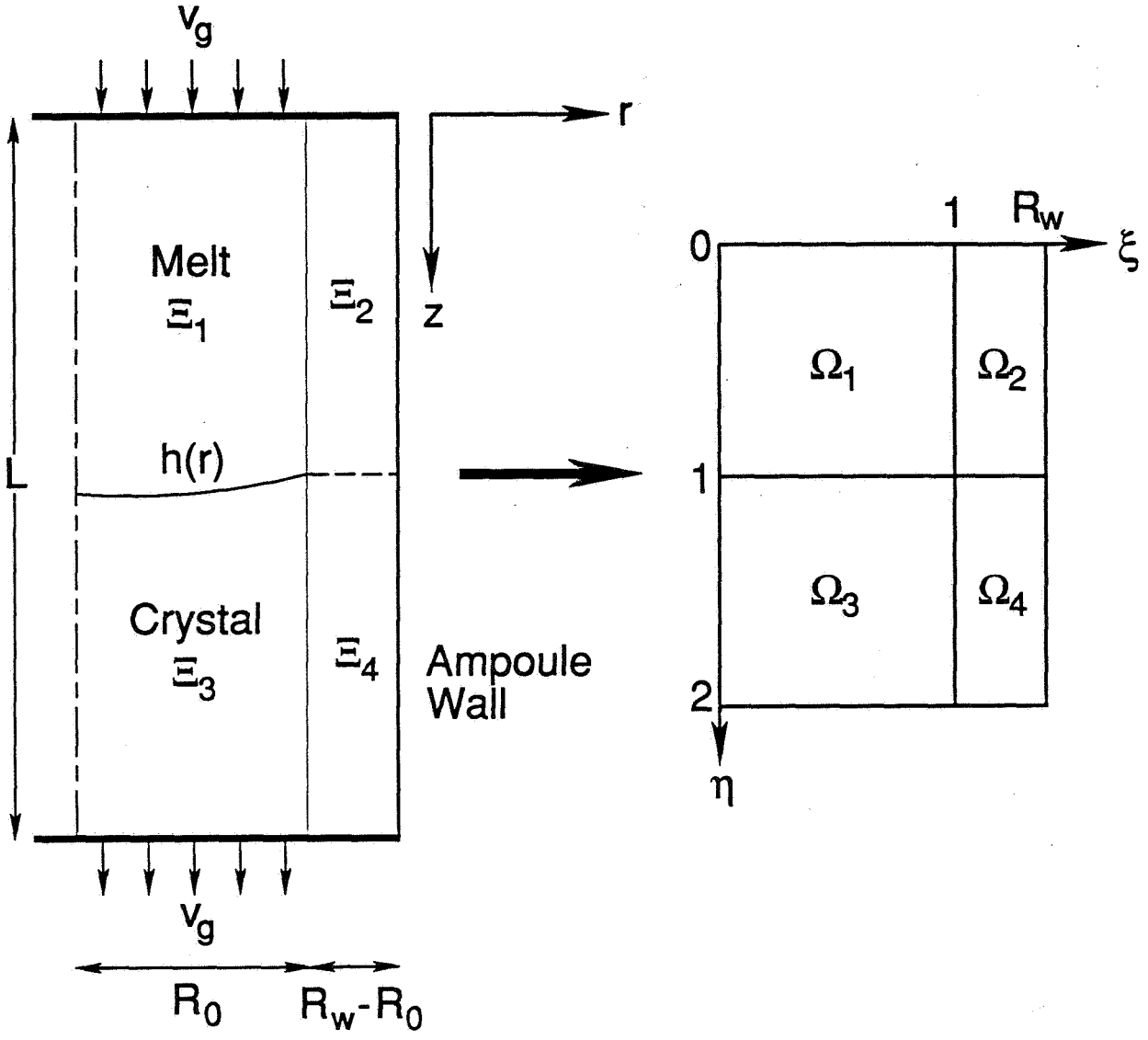
v_g
r
Melt
Ξ_1
Ξ_2
z
L
h(r)
Crystal
Ξ_3
Ξ_4
Ampoule
Wall
v_g
R_0
R_w-R_0
0
1
R_w
ξ
Ω_1
Ω_2
1
Ω_3
Ω_4
2
η

FIG. 2

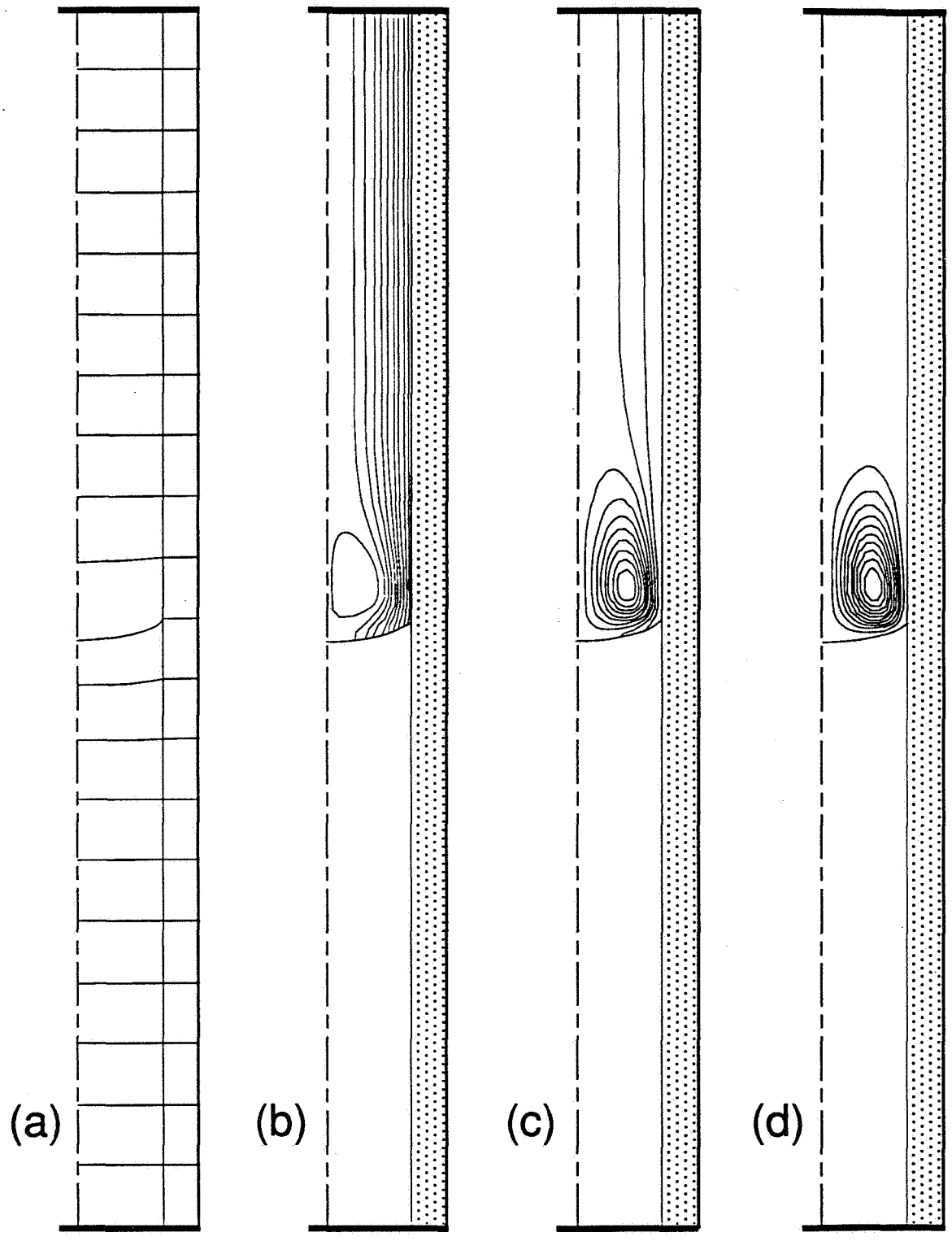

FIG. 3

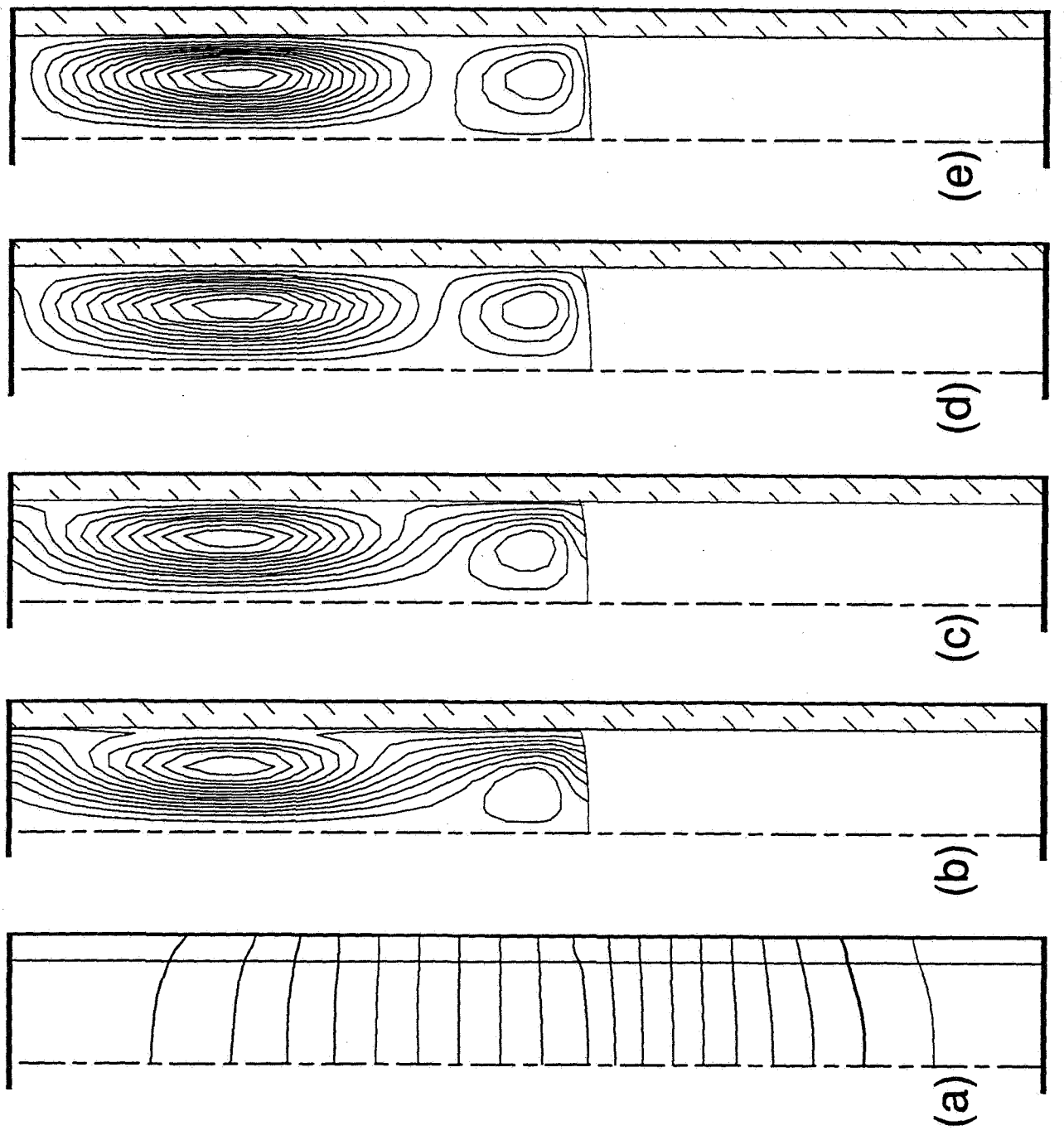

FIG. 4

machine	compiler options	cpu time (sec)	number of outer iterations	number of inner iterations for each outer loop									
cray XMP/24	vector, double precision	1157	10	1501	340	247	190	174	150	111	87	103	94
ipsc (1 node)	vector, double precision and maximum optimization	8076	10	613	1342	268	275	236	174	156	151	29	65
Ardent Titan II 2 CPU's	vector, parallel, double precision and maximum optimization	11015	10	613	1342	268	275	236	174	156	151	29	65

Table 1: Comparison of CPU times for different machines for the Gr = case using our method.